Role of enthalpy of formation on lattice distortion and intrinsic ductility of concentrated refractory alloys

Sufyan M. Shaikh[a,b], B. S. Murty[c], Satyesh K. Yadav[a,b,*]

[a]Department of Metallurgical and Materials Engineering, Indian Institute of Technology Madras, Chennai, 600036, Tamil Nadu, India
[b]Center for Atomistic Modelling and Materials Design, Indian Institute of Technology Madras, Chennai, 600036, Tamil Nadu, India
[c]Materials Science & Metallurgical Engineering, Indian Institute of Technology Hyderabad, Kandi, 502285, Telangana, India

Abstract

Valence electron concentration (VEC), Pugh's ratio (B/G), lattice distortion (δ), and intrinsic ductility (D) are few of the empirical parameters widely used to design ductile refractory alloys. However, the D is the only parameter which considers the relative competition between cracking (surface energy, γ_s) and the barrier to dislocation motion (unstable stacking fault energy, γ_{usfe}). Here we studied the enthalpy of formation (ΔE_f), Root-mean-squared Lattice Distortion (RLD), and D of 9 refractory metals and 36 equiatomic refractory alloys using density functional theory simulations. A sinusoidal formulation of barrier to the glide of slip planes based on γ_{usfe} has been developed. A strong inverse correlation between D and the maximum barrier to slip plane glide has been found. We found that the dislocation core width is not influenced by the γ_{usfe} of refractory metals. The RLD is 9% of the dislocation core width, which may not be large enough to affect the dislocation line. However, the local ΔE_f variation along the dislocation line influences the local γ_{usfe}, leading to a wavy dislocation line. We found that positive ΔE_f and atomic size difference leads to RLD, which does not necessarily require large compositional complexity as of high-entropy alloys. The D and the barrier to slip plane glide correctly captures the experimentally observed ductility in refractory alloys. We found that the success of VEC, lattice distortion, and D in designing ductile refractory alloys was dependent on the underlying ΔE_f of the alloy. Here we provide a universal method to design a ductile refractory alloys which can be thermodynamically stable.

Keywords: Ab initio calculations, Enthalpy of formation, Interfaces (twin boundaries, stacking faults), Stacking-fault energy, High-entropy alloys, Metal and alloys, Shear planes

1. Introduction

Development of alloys for high-temperature applications require one to study a large number of alloys on variety of properties to come up with right composition. Recently, refractory high-entropy alloys (RHEA) have been widely looked into as the candidate material for many high-temperature applications [1]. The high-entropy concept ensures that there is no solute and solvent in the solid solution [2]. Designing a ductile RHEA for such applications requires one to study a large number of alloying elements and their effect on the base alloy [3]. The resulting composition explosion as we move towards the center of the phase diagram requires a well-defined strategy to down-select alloys from such a large composition space [4].

The large difference between the atomic sizes of the constituent atoms has been reported to result in large lattice distortion (LD) in high-entropy alloys (HEA) [5, 6, 7, 8, 9]. The LD in HEA has been reported to alter the dislocation pathways [10], leading to solid solution strengthening in HEA [11, 12]. Here we report that the large LD may not be exclusive to HEA alone, and it can occur in binary alloys as well. Decreasing the valence electron concentration (VEC) has been shown to ductilize RHEA [13]. The VEC criteria is not applicable in WRe alloys where high valency Re is added to ductilize low valency W. The LD and VEC are two inherent parameters used to design intrinsically ductile RHEA. These parameters are used to explain and design very narrow alloy chemistries. However, there is a lack of universal design parameter which is not specific to any system.

Most RHEA have body centered cubic (BCC) crystal structure as majority of their constituent elements are BCC. Understanding the deformation mechanism in BCC alloys have remained a challenge due to the temperature dependent activation of multiple slip systems. Pugh's ratio [14], Rice-Thompson parameter [15, 16, 17], intrinsic ductility (D) [18] are the parameters proposed in the literature to assess the ductility of refractory alloys. The Pugh's ratio is directly borrowed from FCC pure metals [14]. The Rice-Thompson parameter and the D discusses the competition between the energy cost of creating new crack surface and the barrier to dislocation motion. Here we used the enthalpy of formation (ΔE_f) and the change in unstable stacking fault energy over its composition av-

*Corresponding author: satyesh@iitm.ac.in

eraged value ($\Delta\gamma_{usfe}$) to down-select ternary, quaternary, and quinary alloys with a goal of developing a ductile RHEA.

2. Methods

Based on our earlier observations on the effect of ΔE_f on the γ_{usfe} of binary equiatomic refractory alloys [19], we selected 6 ternary, 3 quaternary, and 2 quinary equiatomic refractory alloys. The alloy selection methodology is shown in Figure 1. Lattice parameter (a, Å), enthalpy of

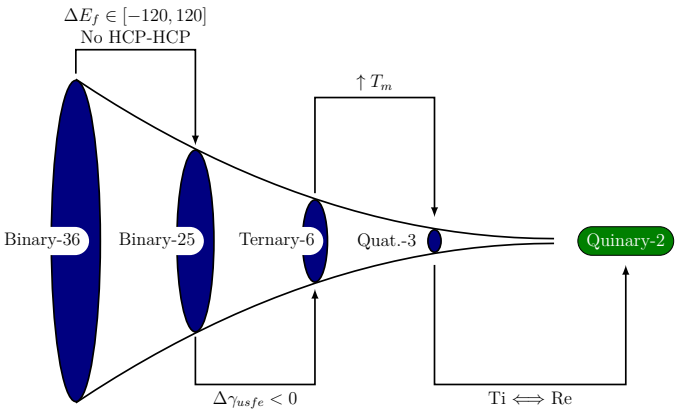

Figure 1: Alloy design process. The funnel signifies reduced composition space as we move forward in the alloy development stages, preventing the composition explosion as we move to higher order systems. The numbers at every stage indicates the number of alloys studied.

formation (ΔE_f, meV/Atom), unstable stacking fault energy (γ_{usfe}, mJ/m^2), surface energy (γ_s, mJ/m^2), intrinsic ductility parameter (D=γ_s/γ_{usfe}), composition averaged melting point (T$_m$, K) [20], Root-mean-squared Lattice Distortion (RLD, Å) [21, 22] are calculated for 25 binary, 6 ternary, 3 quaternary, and 2 quinary equiatomic refractory alloys made from Ti, Zr, Hf, V, Nb, Ta, Mo, W, and Re. The values for ternary, quaternary, and quinary alloys are given in Table 1. The values for pure metals and binary equiatomic refractory alloys are taken from [19]. The γ_s is calculated for {110} plane and γ_{usfe} is calculated for {110}<111> slip system of BCC crystal structure. The ΔE_f is calculated for BCC crystal structure of the alloys. The procedure to calculate γ_s, γ_{usfe}, D, and ΔE_f is given in [19]. The heatmaps and graphs are drawn using Gnuplot [23]. The charge on each atom is calculated using the Bader charge analysis as given in [24, 25, 26, 27] with the post-processing of the charge files done using the code given at [28].

2.1. Special Quasirandom Structures

Special quasirandom structures (SQS) are used to capture chemical disorder in the alloys. SQS are generated using MCSQS code from Alloy Theoretic Automatic Toolkit (ATAT) [29, 30] with pair, triplet, and quadruplet correlations with cut-off distance equal to the BCC unit cell lattice parameter (second nearest neighbor-2NN distance). Ternary, quaternary, and quinary alloys were studied with SQS having 120, 120, and 150 atoms, respectively. The SQS supercell for ternary and quaternary alloys were generated with in-plane dimensions equal to 4 and 3 times of the first nearest neighbor (1NN) distance of the BCC unit cell. Similarly, the SQS supercell for quinary alloys were generated with in-plane dimensions equal to 5 and 3 times of the 1NN distance of the BCC unit cell. The z-axis of SQS supercell was aligned with [110] direction with 10 slip planes of (110) type. A vacuum of 10Å is added to prevent interactions due to periodic boundary condition. The slabs were manipulated using Atomsk [31] and visualized using VESTA [32].

2.2. First-principles calculations

The density functional theory (DFT) simulations were performed using Vienna Ab-initio Simulation Package (VASP) with plane-wave basis and projector augmented wave (PAW) pseudopotentials [33, 34, 35]. For all calculations, a plane wave kinetic energy cutoff of at least 1.3 times the maximum given in the pseudopotential file was used. The electronic exchange-correlation effects were calculated by Perdew-Burke-Erzernhoff generalized gradient approximation (PBE-GGA) [36, 37]. Methfessel-Paxton smearing method with 0.2 eV smearing width was used [38]. Structural relaxation was terminated when the forces on atoms become less than 1 meV/Å. Tetrahedron method with Blöch correction was used for energy calculation [34]. The Brillouin zone sampling was performed using Monkhorst–Pack [39] scheme with automatically generated mesh with k-point spacing of less than $2\pi \times 0.03$ Å^{-1}.

3. Results & discussions

The ternary, quaternary, and quinary equiatomic refractory alloys are selected with an expectation that they will lead to large negative $\Delta\gamma_{usfe}$ when their respective binary equiatomic sub-systems have positive ΔE_f [19]; leading to a positive ΔE_f in the final alloy as well. The alloys studied in present work are listed in Table 1 and in supplementary information file. The VNbTaWRe (ΔE_f=-125.8 meV/Atom) is selected to study the intrinsic ductility of VNbTaWTi when Ti is replaced by Re. Since Ti is susceptible to O absorption [40, 41], therefore replacing Ti with Re is expected to show better oxidation resistance of the quinary alloy. The oxidation susceptibility analysis of refractory alloys is the subject of our future study.

3.1. Intrinsic ductility

3.1.1. Parameter selection for intrinsic ductility

The intrinsic ductility parameter D has been widely used to compare the expected experimental ductility of refractory alloys [42, 43, 44]. The D compares the competition between the energy cost of creating a new crack surface via

Table 1: Alloys under study. The raw data is given in supplementary file. (a - Lattice parameter, Å); γ_s - Surface energy, mJ/m^2; γ_{usfe} - Unstable stacking fault energy, mJ/m^2; $\Delta\gamma_{usfe}$ - % change in γ_{usfe} over its composition average value; D - Intrinsic ductility parameter, (γ_s/γ_{usfe}); T_m - Composition averaged melting point (K); RLD - Root-mean-squared Lattice Distortion, Å; ΔE_f-Enthalpy of formation, meV/Atom)

Alloy	a	γ_s	γ_{usfe}	$\Delta\gamma_{usfe}$	D	T_m	RLD	ΔE_f
VNbTi	3.332	2088	491	-19	4.25	2291	0.098	66.0
VNbW	3.164	2506	1008	-8	2.49	2876	0.059	10.2
VNbMo	3.156	2391	1046	-1	2.29	2610	0.062	-25.9
VNbTa	3.231	2177	631	-5	3.45	2741	0.080	60.9
NbWRe	3.194	2823	1476	10	1.91	3299	0.035	-69.3
MoWRe	3.143	3097	1156	-27	2.68	3348	0.024	55.9
VNbTaW	3.202	2449	967	0	2.53	2980	0.061	8.9
VNbTaTi	3.220	2081	560	-12	3.72	2541	0.086	65.6
VNbTiW	3.177	2281	783	-13	2.91	2642	0.076	29.6
VNbTaWTi	3.206	2237	704	-19	3.18	2772	0.067	32.7
VNbTaWRe	3.175	2735	1367	26	2.00	3074	0.050	-125.8

γ_s and the barrier to dislocation motion via γ_{usfe}. Therefore, an alloy having large D is expected to show better ductility than an alloy having lower D value (Figure 2a).

The ductility of an alloy can also be dictated by their barrier to dislocation motion/glide of slip planes. The barrier to glide of slip planes planes can be found using the sinusoidal formulation of γ_{usfe} curve as shown in Equation (1).

$$\gamma = \gamma_{usfe} \sin^2\left(\frac{\pi x}{b}\right) \tag{1}$$

The maximum of $[\partial\gamma/\partial x]$ occurs at $x = (b/4)$. From Equation (1),

$$\left[\frac{\partial\gamma}{\partial x}\right]_{x=\frac{b}{4}} = \frac{2\pi\gamma_{usfe}}{a\sqrt{3}} \tag{2}$$

A strong inverse correlation has been found between the experimentally observed ductility and $[\partial\gamma/\partial x]$ (Figure 2b). Therefore the $[\partial\gamma/\partial x]$ can be an accurate representation of reality. The D and $[\partial\gamma/\partial x]$ correctly capture the experimentally observed ductility in refractory alloys (Figure 2). Here we used D to design a ductile RHEA based on binary, ternary, and quaternary alloy data.

3.1.2. Improving D

The improvement in D($=\gamma_s/\gamma_{usfe}$) requires low γ_{usfe} and high γ_s. The change in γ_{usfe} over its composition averaged value ($\Delta\gamma_{usfe}$, %) is an important parameter in affecting the change in D. A large negative $\Delta\gamma_{usfe}$ can help in reducing the barrier to dislocation motion or it can assist in glide of slip planes. We observe that a positive ΔE_f leads to a negative $\Delta\gamma_{usfe}$ for the studied equiatomic refractory alloys (Figure 3). Based on our earlier findings of binary equiatomic refractory alloys [19], the positive ΔE_f leads to a large negative $\Delta\gamma_{usfe}$, i.e. the ΔE_f strongly influences the $\Delta\gamma_{usfe}$ (Figure 3). The largest ΔE_f occurs at equiatomic stoichiometry, therefore the largest $\Delta\gamma_{usfe}$ occurs in equiatomic alloys as schematically explained in Figure 4a. It indicates that the positive ΔE_f helps in increasing the D (via negative $\Delta\gamma_{usfe}$) leading to improvement in ductility of presently studied refractory alloys. The entire

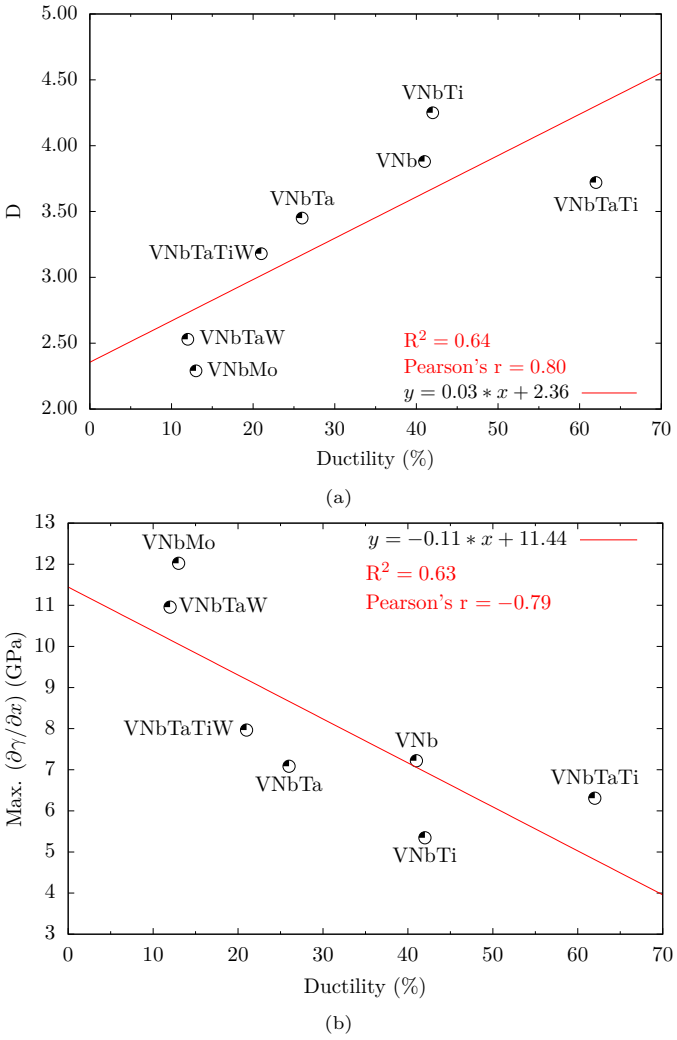

Figure 2: Comparison between experimentally observed ductility of equiatomic refractory alloy and (a)D and (b)Max. $[\partial\gamma/\partial x]$. The D and max.$[\partial\gamma/\partial x]$ can be used to differentiate between intrinsically ductile and intrinsically brittle alloys. Experimental ductility values are taken from [45, 46, 47].

process can be represented as,

$$120 \text{ meV/Atom} \geq \Delta E_f \geq 0 \implies \Delta\gamma_{usfe} << 0 \implies \uparrow \text{D} \implies \text{Better ductility}$$

Therefore ΔE_f can be a useful parameter for selecting the alloying elements for improving the ductility of refractory alloys via increased D. The improvement in D requires negative $\Delta\gamma_{usfe}$ which is strongly influenced by ΔE_f as observed in Figure 3. Therefore the alloying elements should be selected to have a positive ΔE_f.

The ΔE_f of an alloy plays an important role in dictating its thermodynamic stability. From Figure 1, the alloys can be selected for further thermodynamic and microstructural stability studies based on the enthalpy of formation of their constituent phases. The VNbTaWRe alloy have much lower ΔE_f (-125.8 meV/Atom) than VNbTaWTi (ΔE_f= 32.7 meV/Atom). Therefore the Re-containing quinary alloy shows large increase in the γ_{usfe} over its composition

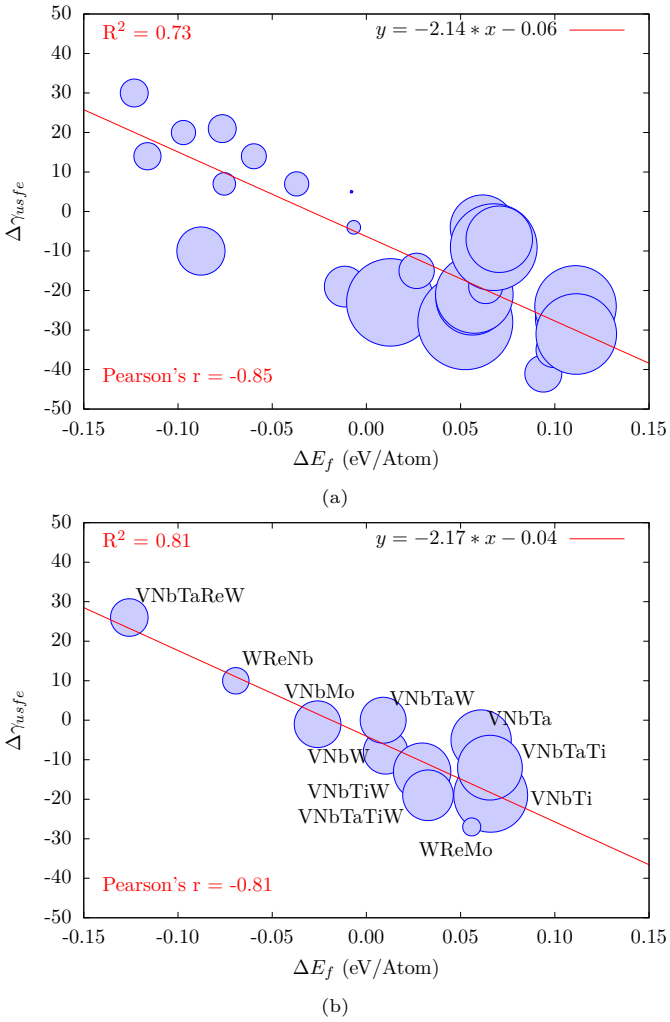

Figure 3: Percentage change in γ_{usfe} as compared to the composition averaged value ($\Delta\gamma_{usfe}$) vs enthalpy of formation (ΔE_f): (a)Binaries (b)Higher order systems. The circle size indicate Root-mean-squared Lattice Distortion (RLD). Positive ΔE_f leads to negative $\Delta\gamma_{usfe}$ and increased RLD.

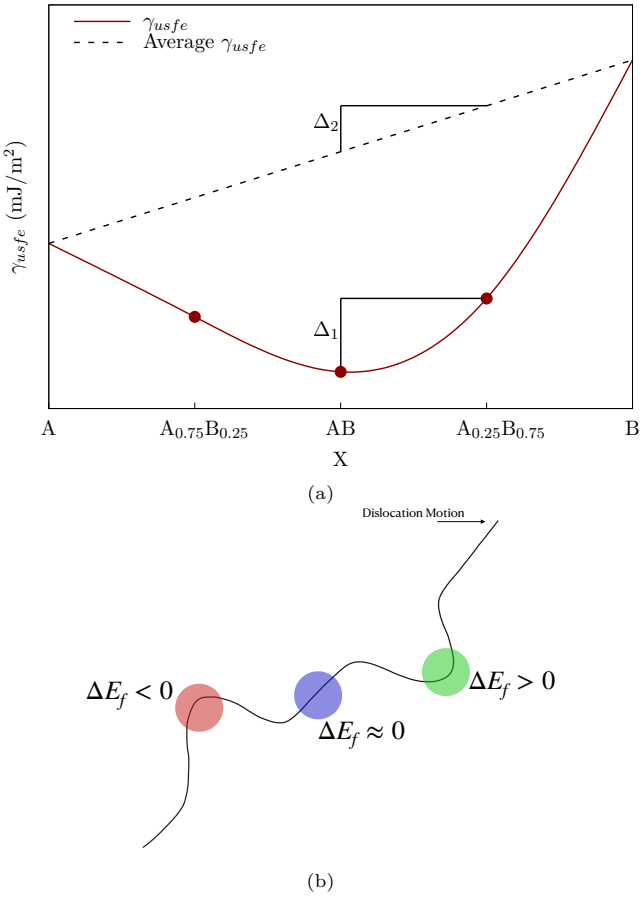

Figure 4: Schematic representation of the change in γ_{usfe} which is greater than that in composition average value. The highest change occurs at the equiatomic composition. (a)Alloy with positive ΔE_f having large reduction in γ_{usfe}. (b)ΔE_f variation along the dislocation resulting in wavy dislocation line.

averaged value (Figure 3b). The γ_{usfe} decreases as the ΔE_f of alloys become more positive (Figure 5). Therefore the D is increased as the ΔE_f of alloys becomes more positive (Figure 6). The large negative ΔE_f leads to increased γ_{usfe} and decreased D of the studied quinary alloys (Figure 5). A similar trend has been observed in binary, ternary, and quaternary alloys; some of which are highlighted in Figures 3b, 5, and 6.

3.2. Lattice distortion

In real alloy systems, the atoms are not located at their ideal lattice sites due to different chemical environment present around each of the lattice sites. Here we calculated this deviation from ideality as Root-mean-squared Lattice Distortion (RLD, Å). The RLD is calculated using the relation,

$$RLD = \sqrt{\frac{1}{n \times i}\sum_{n}\sum_{i}(R_n^i - R_0)^2}$$

$$R_0 = \frac{a_0\sqrt{3}}{2},\ R_i \leq 1.10R_0$$

where, R_n^i is the distance between n^{th} atom and its i^{th} 1NN, R_0 is the ideal 1NN distance, a_0 is the bulk lattice parameter of alloy in BCC symmetry, n is the total number of atoms in supercell, and i is the total number of 1NN (8 in BCC). This approach ensures that the negative and positive distortions in the crystal are captured correctly and are not cancelled-out by the opposite signs of either distortions. RLD is calculated using the code given in [21, 22]. The Table 1 and Figure 7 shows the RLD in the form of heat map and its comparison with pure elements' atomic size difference for binary equiatomic refractory alloys. The RLD values for the studied alloys ranges from 0.003Å (MoW) to 0.126Å (ZrMo) (Figure 7a). A general trend is of higher RLD for alloys having large atomic size difference between constituent atoms (Figure 7b). Similarly, the positive ΔE_f leads to increased RLD (larger cir-

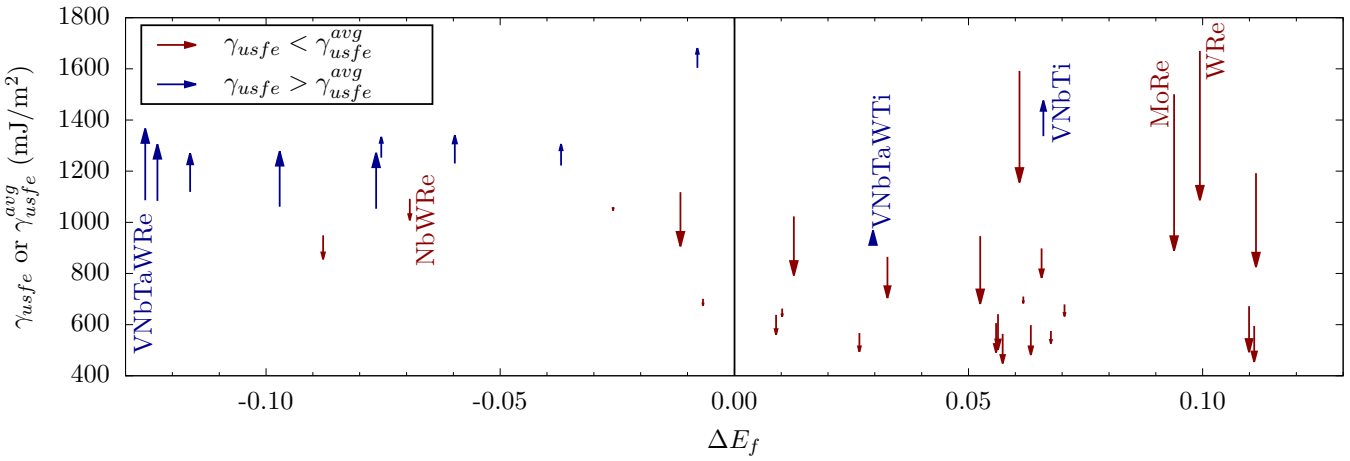

Figure 5: Enthalpy of formation ΔE_f and its influence on unstable stacking fault energy γ_{usfe}. Positive ΔE_f helps in decreasing γ_{usfe} over its composition averaged value γ^{avg}_{usfe}. Replacing Ti with Re in VNbTaWTi leads to large decrease in ΔE_f and large increase in γ_{usfe}. (Arrow base indicates the composition averaged value and arrow head indicates the DFT calculated value.)

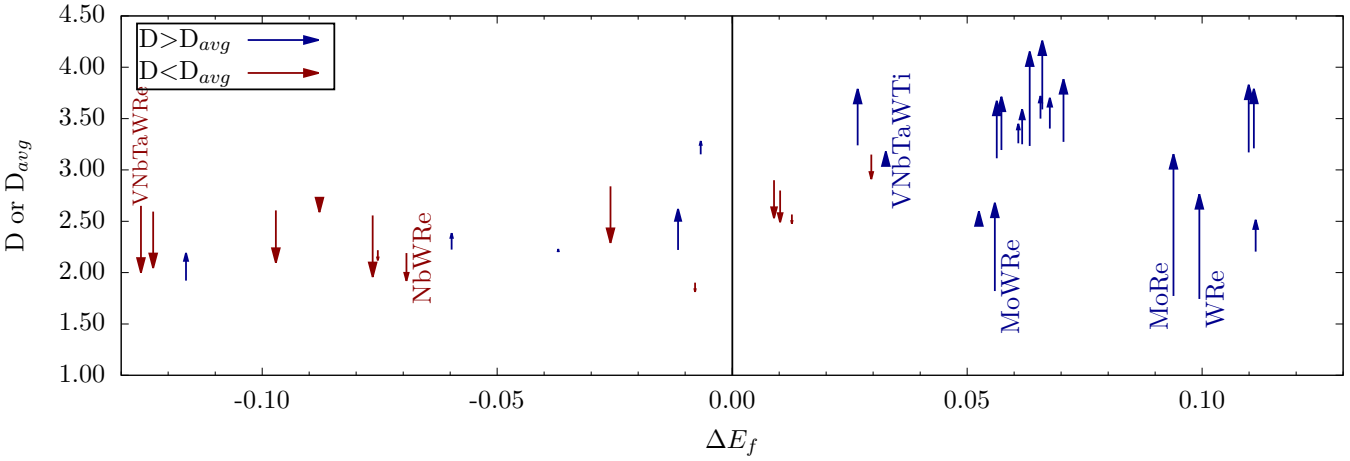

Figure 6: Enthalpy of formation ΔE_f and its influence on intrinsic ductility D. Positive ΔE_f helps in improving D over its composition averaged value D$_{avg}$. Replacing Ti with Re in VNbTaWTi leads to large decrease in ΔE_f and decrease in D. (Arrow base indicates the composition averaged value and arrow head indicates the DFT calculated value.)

cles in Figure 3). This can be attributed to the positive ΔE_f leading to atoms of one element not preferring atoms of different element as their 1NN. A similar RLD is observed in binary (Figure 3a) and in higher-order systems (Figure 3b). Therefore, the RLD is not dependent on the compositional complexity of the system for the presently studied alloys, rather it is dependent on their ΔE_f and atomic size difference. Therefore, to achieve large RLD for specific property requirements, the alloy need not have composition complexity as that in HEA.

A very large positive ΔE_f can lead to large distortions in the crystal and may alter the BCC symmetry of the lattice. Therefore we have put a threshold of ±120 meV/Atom on ΔE_f. This criteria ensure that the alloys remain in BCC symmetry with minimum lattice distortion. Alloys having ΔE_f<-120 meV/Atom are not considered in present study as they may form ordered intermetallics which could be brittle. Similarly, alloys having ΔE_f>120 meV/Atom are not considered in the present study as they may not remain as a stable solid solution (phase separate).

The dislocation core width in BCC crystals is not affected by their γ_{usfe} [48, 49]. The dislocation core width can be defined as ±b/4 [48], where $\bar{b}$=(a/2)<111> is the Burgers vector in BCC crystals. The calculated dislocation core width of the presently studied alloys ranges from 1.33Å (VMo) to 1.49Å (NbZr) (supplementary file). The highest RLD is about 9% of the widest dislocation core. The wavy nature of dislocation line has been shown to occur due to local chemistry changes [50] and short-range ordering/local chemical ordering leading to fluctuations in γ_{sfe} along the dislocation line [51]. Therefore, a wavy dislocation line in HEA can be attributed to the local ΔE_f changes instead of lattice distortion (Figure 4b). However, this claim needs further study of the dislocation core which is beyond the scope of the present work.

From Figures 3 and 8, the RLD is high when the alloys are made from atoms having large atomic size difference for ΔE_f>0. However, for alloys with ΔE_f<0, the mutual

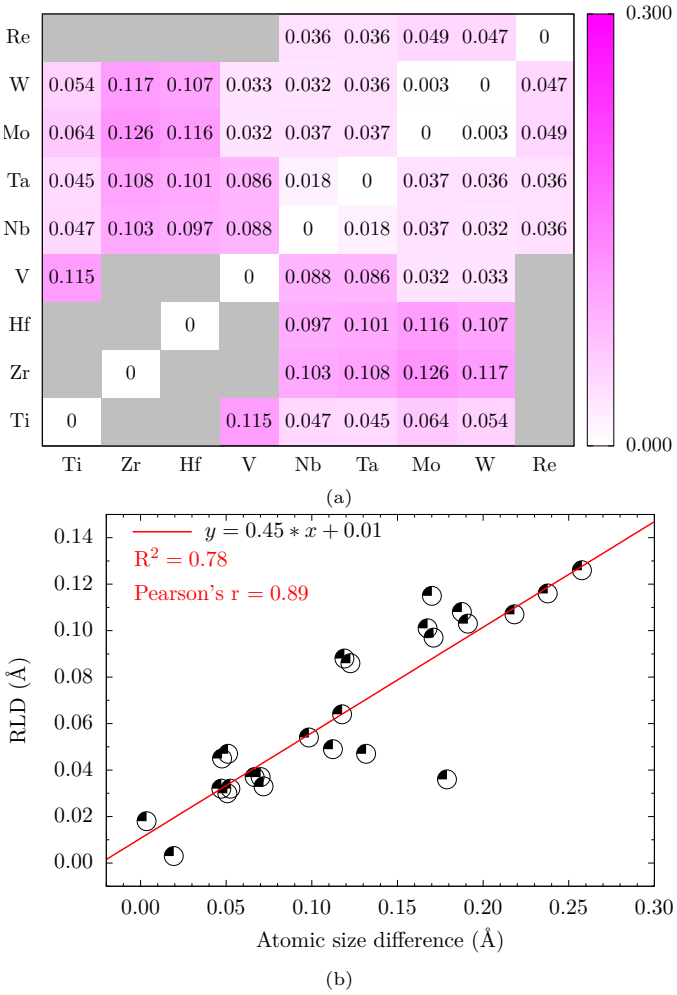

Figure 7: Binary equiatomic refractory alloys. (a)Root mean squared lattice distortion (RLD). (b)Initial atomic size difference strongly influences the RLD. (Atomic radii are calculated from their pure state lattice parameters.)

attraction between atoms led to decreased RLD due to charge transfer. For NbRe (ΔE_f=-116.2 meV/Atom) the charge transfer per atom was 0.627 and the RLD was 0.036 Å. For ZrMo (ΔE_f=52.5 meV/Atom) the charge transfer per atom was 0.646 and the RLD was 0.126 Å. We observe a similar charge transfer but a large RLD for these two extreme cases of ΔE_f. Therefore, a positive ΔE_f is a predominant factor in dictating the RLD in presently studied refractory alloys, irrespective of their compositional complexity.

4. Conclusion

Here we used DFT simulations to calculate the ΔE_f, D, RLD, and $[\partial\gamma/\partial x]$ of 25 binary, six ternary, three quaternary, two quinary equiatomic refractory alloys and nine refractory metals. We found that the ΔE_f strongly influences the intrinsic ductility of alloys. The negative ΔE_f indicates attractive nature of the bonding between constituent atoms and vice-versa. Here we have shown that

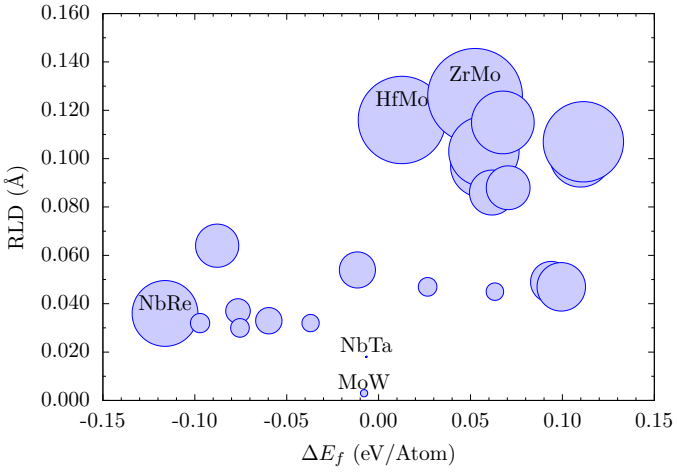

Figure 8: Root-mean-squared lattice distortion (RLD) vs. enthalpy of formation (ΔE_f) in equiatomic binary refractory alloys. Large positive ΔE_f leads to increased RLD. Large atomic size difference between pure metal constituents increases the RLD. (Circle size indicate the atomic size difference. Atomic sizes are calculated from their pure state lattice parameters.)

the positive ΔE_f leads to reduced γ_{usfe} (compared to the composition averaged value) due to the repulsive interaction between the alloy constituents. The maximum reduction in γ_{usfe} could be achieved for alloys having positive ΔE_f which should be well compensated by a sufficiently large entropy.

The RLD increases with ΔE_f. The RLD is at maximum 9% of the widest dislocation core which may not be sufficient to affect the dislocation core. Therefore the wavy nature of dislocation in HEA can be attributed to the large local enthalpy variation rather than the lattice distortion. However, it needs further evaluation of the dislocation core along the dislocation line to better understand the local enthalpy changes due to chemistry variation along the dislocation line. To the best of our knowledge, this is the first time where a local ΔE_f has been used as an indicator of the wavy dislocation line. The calculated max. $[\partial\gamma/\partial x]$ correlates well with the experimentally observed ductility in some of the presently studied concentrated refractory alloys. With the presently developed approach, the number of alloy to be studied (experimentally and/or theoretically) can be drastically reduced as we move from binary to ternary to quaternary to quinary alloys. Here we have reduced the number of alloys to be studied from 84 to 6 in ternary, 126 to 3 in quaternary, and 126 to 2 in quinary alloys, based on the primary goal of increased D and optimum ΔE_f as we move to higher-order systems. Taking the effect of ΔE_f and $[\partial\gamma/\partial x]$ on the deformability of concentrated refractory alloys is likely to open new directions in the design of ductile refractory alloys with appropriate lattice distortion for high-temperature applications.

References

[1] J.-W. Yeh, Recent progress in high-entropy alloys, Ann. Chim. Sci. des Matériaux 31 (6) (2006) 633–648. doi:10.3166/acsm.31.633-648.
URL http://acsm.revuesonline.com/article.jsp?articleId=9099

[2] B. S. Murty, J. W. Yeh, S. Ranganathan, P. P. Bhattacharjee, 2 - High-entropy alloys: basic concepts, in: B. S. Murty, J. W. Yeh, S. Ranganathan, P. P. Bhattacharjee (Eds.), High-Entropy Alloy. (Second Ed., second edi Edition, Elsevier, 2019, pp. 13–30. doi:https://doi.org/10.1016/B978-0-12-816067-1.00002-3.
URL http://www.sciencedirect.com/science/article/pii/B9780128160671000023

[3] D. Miracle, O. Senkov, A critical review of high entropy alloys and related concepts, Acta Mater. 122 (2017) 448–511. doi:10.1016/j.actamat.2016.08.081.
URL http://dx.doi.org/10.1016/j.actamat.2016.08.081

[4] M. Baker, Defining Pathways for Realizing the Revolutionary Potential of High Entropy Alloys: A TMS Accelerator Study, Tech. rep. (oct 2021). doi:10.7449/HEApathways.
URL https://www.tms.org/HEApathways

[5] H. Song, F. Tian, Q. M. Hu, L. Vitos, Y. Wang, J. Shen, N. Chen, Local lattice distortion in high-entropy alloys, Phys. Rev. Mater. 1 (2) (2017) 1–8. doi:10.1103/PhysRevMaterials.1.023404.

[6] Y. Tong, S. Zhao, H. Bei, T. Egami, Y. Zhang, F. Zhang, Severe local lattice distortion in Zr- and/or Hf-containing refractory multi-principal element alloys, Acta Mater. 183 (2020) 172–181. doi:10.1016/j.actamat.2019.11.026.
URL https://doi.org/10.1016/j.actamat.2019.11.026

[7] Z. An, S. Mao, Y. Liu, L. Wang, H. Zhou, B. Gan, Z. Zhang, X. Han, A novel HfNbTaTiV high-entropy alloy of superior mechanical properties designed on the principle of maximum lattice distortion, J. Mater. Sci. Technol. 79 (2021) 109–117. doi:10.1016/j.jmst.2020.10.073.
URL https://doi.org/10.1016/j.jmst.2020.10.073https://linkinghub.elsevier.com/retrieve/pii/S1005030220310112

[8] S. S. Sohn, A. Kwiatkowski da Silva, Y. Ikeda, F. Körmann, W. Lu, W. S. Choi, B. Gault, D. Ponge, J. Neugebauer, D. Raabe, Ultrastrong Medium-Entropy Single-Phase Alloys Designed via Severe Lattice Distortion, Adv. Mater. 31 (8) (2019) 1807142. doi:10.1002/adma.201807142.
URL https://onlinelibrary.wiley.com/doi/10.1002/adma.201807142

[9] W. Lai, F. Vogel, X. Zhao, B. Wang, Y. Yi, D. You, X. Tong, W. Li, X. Yu, X. Wang, Design of BCC refractory multi-principal element alloys with superior mechanical properties, Mater. Res. Lett. 10 (3) (2022) 133–140. doi:10.1080/21663831.2021.2024615.
URL https://doi.org/10.1080/21663831.2021.2024615

[10] E. Ma, Unusual dislocation behavior in high-entropy alloys, Scr. Mater. 181 (2020) 127–133. doi:10.1016/j.scriptamat.2020.02.021.
URL https://doi.org/10.1016/j.scriptamat.2020.02.021

[11] H. Chen, A. Kauffmann, S. Laube, I.-C. Choi, R. Schwaiger, Y. Huang, K. Lichtenberg, F. Müller, B. Gorr, H.-J. Christ, M. Heilmaier, Contribution of Lattice Distortion to Solid Solution Strengthening in a Series of Refractory High Entropy Alloys, Metall. Mater. Trans. A 49 (3) (2018) 772–781. doi:10.1007/s11661-017-4386-1.
URL http://link.springer.com/10.1007/s11661-017-4386-1

[12] C. Lee, G. Song, M. C. Gao, R. Feng, P. Chen, J. Brechtl, Y. Chen, K. An, W. Guo, J. D. Poplawsky, S. Li, A. T. Samaei, W. Chen, A. Hu, H. Choo, P. K. Liaw, Lattice distortion in a strong and ductile refractory high-entropy alloy, Acta Mater. 160 (2018) 158–172. doi:10.1016/j.actamat.2018.08.053.

[13] S. Sheikh, S. Shafeie, Q. Hu, J. Ahlström, C. Persson, J. Veselý, J. Zýka, U. Klement, S. Guo, Alloy design for intrinsically ductile refractory high-entropy alloys, J. Appl. Phys. 120 (16) (2016) 164902. doi:10.1063/1.4966659.
URL http://aip.scitation.org/doi/10.1063/1.4966659

[14] S. Pugh, XCII. Relations between the elastic moduli and the plastic properties of polycrystalline pure metals, London, Edinburgh, Dublin Philos. Mag. J. Sci. 45 (367) (1954) 823–843. doi:10.1080/14786440808520496.
URL http://www.tandfonline.com/doi/abs/10.1080/14786440808520496

[15] J. R. Rice, R. Thomson, Ductile versus brittle behaviour of crystals, Philos. Mag. A J. Theor. Exp. Appl. Phys. 29 (1) (1974) 73–97. doi:10.1080/14786437408213555.
URL https://www.tandfonline.com/doi/full/10.1080/14786437408213555

[16] J. R. Rice, Dislocation nucleation from a crack tip: An analysis based on the Peierls concept, J. Mech. Phys. Solids 40 (2) (1992) 239–271. doi:10.1016/S0022-5096(05)80012-2.
URL https://linkinghub.elsevier.com/retrieve/pii/S0022509605800122

[17] J. R. Rice, G. E. Beltz, The activation energy for dislocation nucleation at a crack, J. Mech. Phys. Solids 42 (2) (1994) 333–360. doi:10.1016/0022-5096(94)90013-2.

[18] U. V. Waghmare, E. Kaxiras, V. V. Bulatov, M. S. Duesbery, Effects of alloying on the ductility of MoSi 2 single crystals from first-principles calculations, Model. Simul. Mater. Sci. Eng. 6 (4) (1998) 493–506. doi:10.1088/0965-0393/6/4/013.
URL https://iopscience.iop.org/article/10.1088/0965-0393/6/4/013

[19] S. M. Shaikh, B. Murty, S. K. Yadav, Designing a thermodynamically stable and intrinsically ductile refractory alloy, J. Alloys Compd. 939 (2023) 168597. arXiv:2203.09949, doi:10.1016/j.jallcom.2022.168597.
URL https://linkinghub.elsevier.com/retrieve/pii/S092583882204988X

[20] S. M. Shaikh, V. Hariharan, S. K. Yadav, B. Murty, CALPHAD and rule-of-mixtures: A comparative study for refractory high entropy alloys, Intermetallics 127 (May) (2020) 106926. doi:10.1016/j.intermet.2020.106926.
URL https://doi.org/10.1016/j.intermet.2020.106926

[21] S. M. Shaikh, B. S. Murty, S. K. Yadav, RLD, GitHub (2022).
URL https://github.com/sufyanshk/RLD

[22] J. Blomqvist, vasputil, GitHub (2016).
URL https://github.com/jabl/vasputil

[23] T. Williams, C. Kelley, {Many others}, gnuplot 5.4: an interactive plotting program (2022).
URL http://www.gnuplot.info

[24] G. Henkelman, A. Arnaldsson, H. Jónsson, A fast and robust algorithm for Bader decomposition of charge density, Comput. Mater. Sci. 36 (3) (2006) 354–360. doi:10.1016/j.commatsci.2005.04.010.

[25] W. Tang, E. Sanville, G. Henkelman, A grid-based Bader analysis algorithm without lattice bias, J. Phys. Condens. Matter 21 (8) (2009). doi:10.1088/0953-8984/21/8/084204.

[26] M. Yu, D. R. Trinkle, Accurate and efficient algorithm for Bader charge integration, J. Chem. Phys. 134 (6) (2011) 1–8. arXiv:1010.4916, doi:10.1063/1.3553716.

[27] A.-r. Allouche, Software News and Updates Gabedit — A Graphical User Interface for Computational Chemistry Softwares, J. Comput. Chem. 32 (2012) 174–182. doi:10.1002/jcc.

[28] S. M. Shaikh, B. S. Murty, S. K. Yadav, BaderPostProcess (2023).
URL https://github.com/sufyanshk/BaderPostProcess

[29] A. van de Walle, M. Asta, G. Ceder, The Alloy Theoretic Automated Toolkit: A User Guide, Calphad 26 (4) (2002) 539–553. arXiv:0212159, doi:10.1016/S0364-5916(02)80006-2.

[30] A. van de Walle, Axel van de Walle, A. van de Walle, M. D. Asta, G. Ceder, The Alloy-Theoretic Automated Toolkit (ATAT): A User Guide, Vol. 26, 2013.

[31] P. Hirel, Atomsk: A tool for manipulating and converting atomic data files, Comput. Phys. Commun. 197 (2015) 212–219. doi:https://doi.org/10.1016/j.cpc.2015.07.012.
URL https://www.sciencedirect.com/science/article/pii/S0010465515002817

[32] K. Momma, F. Izumi, VESTA 3 for three-dimensional vi-

sualization of crystal, volumetric and morphology data, J. Appl. Crystallogr. 44 (6) (2011) 1272–1276. doi:10.1107/S0021889811038970.
[33] G. Kresse, J. Hafner, Ab initio molecular dynamics for liquid metals, Phys. Rev. B 47 (1) (1993) 558–561. doi:10.1103/PhysRevB.47.558.
[34] P. E. Blöchl, Projector augmented-wave method, Phys. Rev. B 50 (24) (1994) 17953–17979. doi:10.1103/PhysRevB.50.17953.
[35] G. Kresse, J. Furthmüller, Efficient iterative schemes for ab initio total-energy calculations using a plane-wave basis set, Phys. Rev. B 54 (16) (1996) 11169–11186. doi:10.1103/PhysRevB.54.11169.
[36] J. P. Perdew, K. Burke, M. Ernzerhof, Generalized gradient approximation made simple, Phys. Rev. Lett. 77 (18) (1996) 3865–3868. doi:10.1103/PhysRevLett.77.3865.
[37] D. Joubert, From ultrasoft pseudopotentials to the projector augmented-wave method, Phys. Rev. B - Condens. Matter Mater. Phys. 59 (3) (1999) 1758–1775. doi:10.1103/PhysRevB.59.1758.
[38] M. Methfessel, A. T. Paxton, High-precision sampling for Brillouin-zone integration in metals, Phys. Rev. B 40 (6) (1989) 3616–3621. doi:10.1103/PhysRevB.40.3616.
[39] H. J. Monkhorst, J. D. Pack, Special points for Brillouin-zone integrations, Phys. Rev. B 13 (12) (1976) 5188–5192. doi:10.1103/PhysRevB.13.5188.
URL https://link.aps.org/doi/10.1103/PhysRevB.13.5188
[40] L. Kong, T. Ouchi, C. Zheng, T. H. Okabe, Electrochemical Deoxidation of Titanium Scrap in MgCl 2 -HoCl 3 System , J. Electrochem. Soc. 166 (13) (2019) E429–E437. doi:10.1149/2.1011913jes.
[41] Z. Z. Fang, J. D. Paramore, P. Sun, K. S. Chandran, Y. Zhang, Y. Xia, F. Cao, M. Koopman, M. Free, Powder metallurgy of titanium–past, present, and future, Int. Mater. Rev. 63 (7) (2018) 407–459. doi:10.1080/09506608.2017.1366003.
URL https://doi.org/10.1080/09506608.2017.1366003
[42] X. Li, W. Li, D. L. Irving, L. K. Varga, L. Vitos, S. Schönecker, Ductile and brittle crack-tip response in equimolar refractory high-entropy alloys, Acta Mater. 189 (2020) 174–187. arXiv:2002.07013, doi:10.1016/j.actamat.2020.03.004.
URL https://linkinghub.elsevier.com/retrieve/pii/S1359645420301816
[43] E. Mak, B. Yin, W. Curtin, A ductility criterion for bcc high entropy alloys, J. Mech. Phys. Solids 152 (July 2020) (2021) 104389. doi:10.1016/j.jmps.2021.104389.
URL https://linkinghub.elsevier.com/retrieve/pii/S0022509621000776
[44] O. N. Senkov, D. B. Miracle, Generalization of intrinsic ductile-to-brittle criteria by Pugh and Pettifor for materials with a cubic crystal structure, Sci. Rep. 11 (1) (2021) 10–13. doi:10.1038/s41598-021-83953-z.
URL https://doi.org/10.1038/s41598-021-83953-z
[45] J. P. Couzinié, O. N. Senkov, D. B. Miracle, G. Dirras, Comprehensive data compilation on the mechanical properties of refractory high-entropy alloys, Data Br. 21 (2018) 1622–1641. doi:10.1016/j.dib.2018.10.071.
URL http://dx.doi.org/10.1016/j.dib.2018.10.071
[46] R. Feng, G. Kim, D. Yu, Y. Chen, W. Chen, P. K. Liaw, K. An, Elastic behavior of binary and ternary refractory multi-principal-element alloys, Mater. Des. 219 (2022). doi:10.1016/j.matdes.2022.110820.
[47] Z. Han, L. Meng, J. Yang, G. Liu, J. Yang, R. Wei, G. Zhang, Novel BCC VNbTa refractory multi-element alloys with superior tensile properties, Mater. Sci. Eng. A 825 (July) (2021) 141908. doi:10.1016/j.msea.2021.141908.
URL https://doi.org/10.1016/j.msea.2021.141908
[48] Y. Kamimura, K. Edagawa, S. Takeuchi, Experimental evaluation of the Peierls stresses in a variety of crystals and their relation to the crystal structure, Acta Mater. 61 (1) (2013) 294–309. doi:10.1016/j.actamat.2012.09.059.
URL http://dx.doi.org/10.1016/j.actamat.2012.09.059
[49] Y. Kamimura, K. Edagawa, A. M. Iskandarov, M. Osawa, Y. Umeno, S. Takeuchi, Peierls stresses estimated via the Peierls-Nabarro model using ab-initio γ-surface and their comparison with experiments, Acta Mater. 148 (2018) 355–362. doi:10.1016/j.actamat.2018.02.009.
URL http://dx.doi.org/10.1016/j.actamat.2018.02.009
[50] F. Maresca, W. A. Curtin, Mechanistic origin of high strength in refractory BCC high entropy alloys up to 1900K, Acta Mater. 182 (2020) 235–249. arXiv:1901.02100, doi:10.1016/j.actamat.2019.10.015.
URL https://doi.org/10.1016/j.actamat.2019.10.015
[51] Q. J. Li, H. Sheng, E. Ma, Strengthening in multi-principal element alloys with local-chemical-order roughened dislocation pathways, Nat. Commun. 10 (1) (2019) 1–11. arXiv:1904.07681, doi:10.1038/s41467-019-11464-7.
URL http://dx.doi.org/10.1038/s41467-019-11464-7